Journal of Energy Storage xxx (xxxx) xxx

Contents lists available at ScienceDirect

Journal of Energy Storage

journal homepage: www.elsevier.com/locate/est

Calendar aging model for lithium-ion batteries considering the influence of cell characterization

Amelie Krupp [a,*], Robert Beckmann [a], Theys Diekmann [a], Ernst Ferg [b], Frank Schuldt [a], Carsten Agert [a]

[a] DLR Institute of Networked Energy Systems, Carl-von-Ossietzky-Straße 15, Oldenburg, 26129, Germany
[b] Department of Chemistry and uYilo, e-Mobility Technology Innovation Programme, Nelson Mandela University, P.O. Box 77000, Port Elizabeth, 6001, South Africa

ARTICLE INFO

Keywords:
Lithium-ion battery
Calendar aging
Characterization
Capacity gain
Passive anode effect

ABSTRACT

To optimize costs and ensure safety, investigation and modeling of battery aging is very important. Calendar aging analysis consist of a periodic sequence of calendar aging and cell characterization. The influence of the characterization on the results of the calendar aging investigation has been assumed to be negligible so far. Nevertheless, the characterization measurements of different studies, especially the important capacity measurement, differ fundamentally. This could have an impact on the results of capacity and resistance change in calendar aging. In this paper, the effect of characterization is quantified for the first time, using periodic characterization measurements. A significant influence in the form of capacity increase and resistance decrease is found. It can be explained by an increase in the active electrode surface area caused by the characterization measurement. Therefore, the cell characterization is a new possible source for capacity increase in calendar aging. As an important result, in future studies capacity measurements should be performed with small currents below 1C to reduce the influence of characterization on the results. Additionally, a correction of the characterization effect can be done according to the presented method.

1. Introduction

Diagnosis and prognosis of battery aging is essential not only to ensure safety but also to optimize profitability of battery storage systems. Battery aging can be detected by a decrease in capacity and an increase in internal resistance. In aging models, a distinction is made between calendar aging during rest times of the battery and cyclic aging due to cyclization.

Many approaches exist for modeling battery aging. Theoretical models calculate the aging of batteries based on physical relationships. The model scale varies from macro- to micro-scale, including the modeling of processes at the atomic level. Since a wide variety of aging mechanisms influence the battery aging, these models quickly become complex and require high computing effort. They are particularly suitable for understanding chemical and physical processes within the battery cell. In contrast to that, empirical models are based on a statistical description of measured data. There is no need for knowledge of the processes taking place in the cell. They are usually related to a specific application and limited by the experimental data, which results in a considerable measurement effort. Semi-empirical models represent a hybrid form of these approaches. The model equations are based on theoretical relationships and are parameterized using empirical measurement data. They offer the advantage of lower computational effort and easier parameterization compared to theoretical models. Furthermore, due to the physical background, they can be better extrapolated and require less measurement effort than empirical models [1–3].

In applications with many rest periods or predominant cyclization with small currents and small depth of discharge, the analysis of calendar aging is particularly important. A wide variety of model approaches can be found to describe calendar aging. A literature review on the cell chemistry and target values considered in different semi-empirical aging models is provided in Table 1. It is to be noted that many of the publications included model not only calendar but also cyclic aging, which is not listed separately.

1.1. Battery cell characterization tests

Calendar aging measurements are used to parametrize semi-empirical models. They consist of a periodic sequence of a calendar aging step and a characterization measurement. Battery cell

* Corresponding author.
E-mail address: Amelie.Krupp@dlr.de (A. Krupp).

https://doi.org/10.1016/j.est.2021.103506
Received 31 August 2021; Received in revised form 13 October 2021; Accepted 27 October 2021

Table 1
Literature review on cell chemistry and target value (capacity C and resistance R) of semi-empirical calendar aging models.

Source	Cell chemistry	Target value	
		C	R
Baghdadi et al. 2016 [4]	NCA, NMC	x	x
Ecker et al. 2012 [5]	NMC	x	x
Grolleau et al. 2014 [6]	LFP	x	–
Hahn et al. 2018 [7]	NMC	x	–
Hoog et al. 2017 [8]	NMC	x	–
Marongiu et al. 2015 [9]	NMC, LFP	x	x
Naumann et al. 2018 [10]	LFP	x	x
Rumberg et al. 2020 [11]	NMC	x	x
Schmalstieg et al. 2014 [1]	NMC	x	x
Smith et al. 2012 [12]	NCA	x	x
Xu et al. 2018 [3]	LMO, LFP, NMC	x	–

characterization usually includes a capacity measurement and a pulse test, to determine the cells capacity C and resistance R. Optionally, other supplementary measurements such as an Electrochemical Impedance Spectroscopy (EIS) or charge/discharge cycles at small current rates are added. The latter can be used to perform an Incremental Capacity Analysis (ICA) or Differential Voltage Analysis (DVA).

In the capacity measurement the battery cells are charged and discharged within their maximum voltage range. At the end of charging, after the maximum voltage is reached, typically a Constant Voltage (CV) phase follows until the current reaches a lower limit (mostly 1/20C). This ensures better comparability of the measured capacities since the lithium ions got more time to rearrange in the electrodes. Afterwards, the cells are discharged at Constant Current (CC) to their final discharge voltage to determine the discharge capacity.

The internal resistance is often determined using a pulse test at different states of charge. In this procedure, the cell is charged or discharged to a fixed SOC with a constant current. After a pause, a charge and/or discharge pulse at a high current rate (usually above 1C) follows. When a charge and discharge pulse are performed, a short rest is inserted between them. Under load, the voltage of the battery deviates from the voltage at rest due to voltage drop on the polarization resistance. The polarization resistance is made up of different components that affect the overvoltage on different time scales. The ohmic resistance causes the initial voltage drop. The charge transfer resistance, which is influenced by the double layer capacitance at the border between electrode and electrolyte, produces the flattening voltage drop in the time range of a few seconds. The final voltage drop is provided by the limited diffusion speed of the lithium ions in the electrolyte and the electrode material [13,14]. Accordingly, the pulse time and current determine which and how intense components of the polarization resistance are considered. The resistance is then determined by Eq. (1):

$$R_t = \frac{U_t - U_{t_0}}{I}. \tag{1}$$

Thereby $U_t - U_{t_0}$ is the voltage difference caused by the current I, evaluated after the time t.

Table 2 shows the main components of the characterization measurements used in the calendar aging studies introduced in Table 1, provided they presented detailed information about their measurement process. Performing a capacity measurement is a fundamental commonality of the characterizations listed. However, the individual capacity measurements are significantly different. The most important differences are the number and the current rate of the measurement cycles. Most capacity measurements are performed at a current rate of 1C. Hahn et al. [7] determine the capacity at 1C and at C/10. Since the transport processes in the battery only take place at a limited speed, the capacity increases with decreasing discharge current. In addition to a higher capacity, the C/10 measurement showed fewer outliers compared to the 1C measurement. Furthermore, at a lower current a smaller capacity increase was measured at the beginning of aging. Since both aspects are beneficial for model fitting, Hahn et al. [7] decided to use the C/10 capacity measurement to evaluate the capacity decrease in their calendar aging study. Barai et al. [15] summarized the commonly used charge and discharge current rates in recent literature and international standards in capacity measurements in their discussion of non-invasive characterization methods. Most commonly, the capacity measurement is performed with a current rate of 1C or C/3. The latter is often used in an automotive application context and is adapted to the average discharge current of a cell in a battery electric vehicle [15,16]. Consistent with this, Hoog [8] and Rumberg [11] used a smaller current rate of C/3 in their capacity test.

1.2. Aging mechanism in calendar aging and characterization cycling

The main causes of calendar aging are parasitic reactions between electrolyte and electrode. They can be classified into three categories: anode reactions (electrolyte reduction leads to Solid Electrolyte Interface (SEI) growth), cathode reactions (including electrolyte oxidation and transition metal dissolution), and coupled reactions (e.g. transition metals dissolved from the cathode affect SEI growth at the anode) [11,17]. SEI growth is assumed to be the dominant aging mechanism and causes irreversible decrease in capacity due to loss of lithium inventory. Reversible capacity loss and gain can be caused by the Passive Anode Effect (PAE). Usually, the anode in lithium-ion batteries is oversized for example due to positioning tolerances in manufacturing when stacking electrodes. Furthermore, in double-sided coatings, the externally located anode has no cathode counterpart [18,19]. Thus, the anode is not fully utilized during charging and discharging processes. When potential differences occur between the active and passive part of the anode, lithium ions slowly enter and leave the overhang by diffusion. After lithium ions entered the overhang, they are in the short term not available for cyclization and therefore the cell capacity reversibly decreases. If lithium ions are released from the overhang, the cell capacity increases. The equalization of the lithium-ion concentration in the active and passive part of the anode happens on large time scales in the range of a few days to several months [18,20].

In addition, reversible capacity gain can also be caused by cathodic side reactions, which lead to a reintercalation of lithium ions back into the cathode [11,17].

In contrast to that, during cycling additional aging mechanisms occur due to the expansion and contraction of the electrode materials caused by the lithium-ion (de-) intercalation. Thereby, the current rate that the cell is subjected to has an influence on the dominant aging mechanisms. At cycling with small currents, cracking in the solid electrolyte interface predominates [21]. Concentration gradients in the electrodes are kept to a minimum at low current rates, therefore less internal stress is exerted on individual particles, which reduces cracking in the active material. When cycling with higher current rates cracking in the anode and cathode active material becomes more relevant. Furthermore, the probability of lithium plating increases due to accumulating lithium ions at the anode [22,23]. Interestingly, also the SEI growth rate increases with higher current during cyclization. This can be explained not only by increased fracture and regeneration of the SEI layer, but also by the electrochemistry of diffusion- and migration-limited SEI growth itself [24]. The mentioned aging mechanism typically cause capacity loss and resistance increase. Contrary to this, Dubarry et al. [25] found an improvement in the cell kinetics of high energy cells cycled with current rates higher than C/5. It is likely caused by an increase in the active surface area due to deformation and cracking in the cathode material resulting from volume changes of the electrode particles during lithium-ion insertion and extraction which is referred to by the authors as an 'electrochemical milling' process. With this, the local effective current density decreases, which leads to a smaller voltage polarization at a fixed current rate. As a final result the discharge voltage, which interrupts the discharging process, is reached later and the capacity of the cell increases.

Table 2
Main components of the characterization measurements in calendar aging experiments. For the capacity measurement the charge (ch.) and discharge (disch.) current rate and the number of cycles (cycl.) are shown. For the pulse test pulse time and C-rate of the charge and discharge pulse and the number of SOC steps are listed. The abbreviation n.a. means, that the information was not available in the cited source.

Source	Capacity measurement			Pulse test			Other
	ch.	disch.	cycl.	Pulse time ch/disch	Pulse C-rate ch/disch	SOC steps	
Baghdadi et al. [4]	CC/CV 1C	CC 1C	2	–/n.a.	-/1C	1	Pseudo OCV, EIS
Ecker et al. [5]	CC/CV 1C	CC 1C	1	10 s/18 s	3C/4C	n.a.	EIS
Grolleau et al. [6]	CC/CV 1C	CC 1C	3	720 s/720 s	1C/1C	5	EIS
Hahn et al. [7]	CC/CV 1C and CC/CV 1C	CC 1C and CC $\frac{C}{10}$	3 and 1	–/30 s	–/4C	3	Charge CC/CV $\frac{C}{10}$
Hoog et al. [8]	CC $\frac{C}{3}$	CC $\frac{C}{3}$	3	–	–	–	–
Marongiu et al. [9]	CC/CV 1C	CC 1C	1	n.a.	n.a.	n.a.	–
Naumann et al. [10]	CC/CV 1C	CC 1C	2	10 s/10 s	$\frac{C}{3}/\frac{C}{3}$ and $\frac{2}{3}$C/$\frac{2}{3}$C and 1C/1C	1	EIS, low rate ch/disch
Rumberg et al. [11]	CC/CV $\frac{C}{3}$	CC $\frac{C}{3}$	3	–/18 s	–/3C	1	OCV
Schmalstieg et al. [1]	CC/CV 1C	CC 1C	1	10 s/18 s	1C/2C	9	–

1.3. Open questions in calendar aging studies

Although the characterization measurements in calendar aging studies differ significantly (see Table 2), the influence of characterization on the measured change in battery capacity and resistance was assumed to be negligible so far. However, depending on the choice of measurement settings, the additional aging mechanisms in cycling may significantly affect the loss of capacity and increase in the internal cell resistance that occurs in the calendar aging measurement.

Some findings in published calendar aging studies could so far not be explained by calendar aging mechanisms or the PAE. Rumberg et al. [11] attributed a capacity gain of a cell aged at 10% SOC and 45 °C to the effect of the anode overhang, since the cells were stored at 30% SOC prior to the start of aging. However, they could not relate an observed capacity gain at 25 °C and 100% SOC to the PAE. In this case, capacity should be decreased by absorption of lithium ions through the overhang during calendar aging. Since it was only a single cell behavior, they did not further search for an explanation. Naumann et al. [10] also assumed a superposition of lithium gain from the overhang and lithium loss due to SEI formation as the cause for the observed capacity gain of their calendar aged cells. They further observed a drop in resistance which could not be explained directly with PAE, since no SOC dependence of the effect was found. They assumed the influence of measurement uncertainties as a possible cause. Lewerenz et al. [19] also noted a drop in resistance on LFP cells calendar aged at 25 °C. They suggested that this may be due to better lithium and electrolyte distribution after initial cycling of the cell in the checkup after a long storage period.

In the discussed literature, a decrease in resistance or an increase in capacity was found in calendar aged cells that could not be related to the passive anode effect or calendar aging mechanisms. From this, the central research question of this paper follows:

- Is there a significant effect of the characterization measurement on capacity and resistance in calendar aging studies?

To answer this question, this study focused on quantifying the influence of the characterization on capacity loss during calendar aging of commercial NMC cells. For this purpose, a method was developed using periodic characterization measurements. Considering the effect of the characterization, the reversible and irreversible capacity loss which belongs to the calendar aging was determined. The corrected data are finally used to parameterize a semi-empirical calendar aging model.

2. Material and methods

This section provides a detailed description of the used cells, measurement systems and methods to allow reproduction of the results.

2.1. Cell specification and testing system

The cells studied were commercial Li(NiMnCo)O_2 (NMC)/graphite pouch cells with a nominal capacity of 64 Ah. The voltage limits are 3.0 V minimum and 4.2 V maximum voltage according to the data sheet provided by the manufacturer. The cells were shipped as a module with about 40% SOC and after a few cycles stored at room temperature. For the aging tests they were removed from the module with about 50% SOC. At this time, the cells were three years old and accordingly already pre-aged.

The measurements are performed with a Maccor series 4000 automated test system with 0 A–150 A current and 0 V–8 V voltage range measuring channels. The current error specified by the manufacturer is 0.05% of full scale current ($\Delta I = 0.075$ A), the voltage error is 0.02% of full scale voltage ($\Delta U = 1.6$ mV). During the measurements, the cells were acclimatized at a constant temperature in a Vötsch VC 7018 climatic chamber.

2.2. Error analysis

The error of the capacity loss is calculated using the Gaussian error propagation law for uncorrelated quantities [26]

$$\Delta F = \pm\sqrt{\left(\frac{\delta F}{\delta x}\cdot\Delta x\right)^2 + \left(\frac{\delta F}{\delta y}\cdot\Delta y\right)^2 + \cdots}. \tag{2}$$

Here $F = F(x, y, \ldots)$ is a functional relation between different directly measurable quantities x, y and the error of the corresponding quantity $\Delta x, \Delta y$. According to this, the measurement error of the capacity is calculated over

$$\Delta C = \Delta I \cdot t_c \tag{3}$$

with the capacity measurement time t_c assumed to be error-free. The error of the capacity equals $\Delta C = \pm 0.075$ Ah for a measuring time of one hour. This corresponds to a relative error of 0.1% with respect to the nominal cell capacity of 64 Ah.

2.3. Calendar aging

At the start of the test series a preconditioning was performed. It consisted of five charge and discharge cycles with 1C. This was followed by an initial characterization of the cells. For the investigation of the calendar aging, the cells were charged to a fixed SOC with 1C at 23 °C. The SOC is related to the actual cell capacity C_{act}:

$$SOC\ [\%] = \frac{\int I\,dt}{C_{act}}\cdot 100\%. \tag{4}$$

Subsequently, the cells were climatized for three hours to the defined aging temperature. In calendar aging, they rested for 60 days before a re-characterization was performed. The SOC was not actively corrected, therefore a slight SOC shift occurs during aging due to the

Table 3
Calendar aging test matrix with the number of cells for each storage condition.

Temperature/SOC	50%	70%	90%
23 °C	2	2	2
40 °C	2	2	2

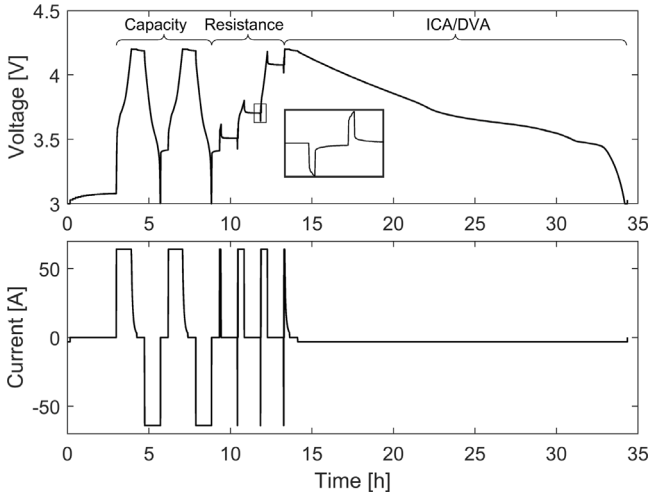

Fig. 1. Voltage and current profile of the characterization over the measurement time.

self-discharge of the cells. Aging was performed at two temperatures (23 °C and 40 °C) and three states of charge (50%, 70% and 90% SOC). Due to the expected Arrhenius dependence of the capacity loss on temperature (see Section 3.4.2), to investigate two temperatures was considered to be sufficient to save measurement resources. Two cells were tested at each test condition to identify possible outliers by considering the expected dependence of the cell aging on the investigated stress factors SOC and temperature. Table 3 shows the test matrix of the twelve calendar aged cells.

2.4. Characterization

The characterization consists of a capacity measurement, a pulse test and a discharge with a small current at 23 °C. In the capacity measurement, the cells were first CC charged with 1C (64 A) to their final charge voltage of 4.2 V. This was followed by a CV phase until the current was less than 1/20C. The cells were then CC discharged with 1C to their final discharge voltage of 3 V to determine the discharge capacity. After each charging and discharging, a 30-min rest followed to allow cell relaxation. The procedure is repeated twice and the second measurement is used to determine the discharge capacity.

The resistance was determined in a Hybrid Pulse Power Characterization (HPPC) test at three SOC (10%, 50% and 90% SOC). Thereby, the cells were first charged with 1C to the smallest SOC. After a one hour rest, a 10 s discharge pulse was performed with 1C. The change in voltage at the beginning and after the end of the pulse was recorded with a high resolution of 10 ms. The cells rested for 60 s before a 10 s charge pulse of 1C was applied. After another 60 s pause, the cells were charged to the next SOC. When the 90% SOC measurement was completed, the cells were fully charged with 1C CC/CV. Finally, after another 30 min rest, a CC discharge with C/10 completes the characterization measurement.

To investigate the influence of the characterization on the calendar aging study, a periodic characterization was performed with two additional cells. It consists of continuous characterizations with a 3 h rest in between. A complete characterization procedure is shown in Fig. 1.

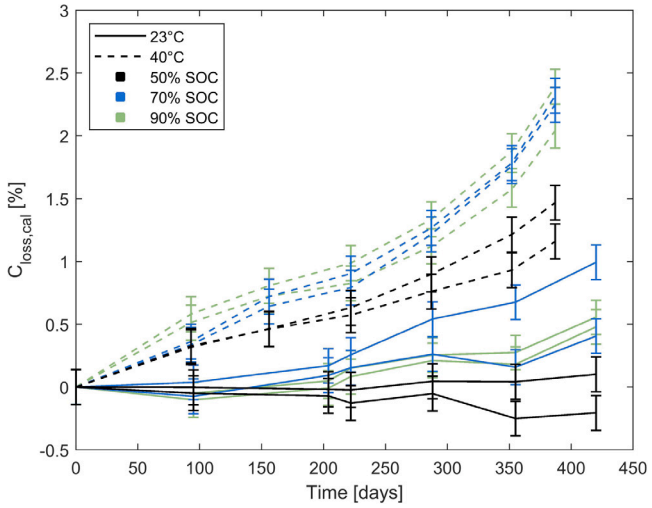

Fig. 2. Relative capacity loss as a function of time for calendar aging at various states of charge and temperatures.

3. Results and discussion

3.1. Aging results

The capacity loss of the batteries during the calendar aging measurement $C_{loss,meas}$ was calculated using

$$C_{loss,meas} = 1 - \frac{C(t)}{C(t_0)} \tag{5}$$

with the cell capacity $C(t)$ at measurement time t and the initial cell capacity $C(t_0)$. Fig. 2 shows the capacity loss of the cells during calendar aging at different states of charge and temperatures. The error intervals are calculated using the Gaussian error propagation law according to Eqs. (5) and (2). They do not fully explain the deviation between the measured values of the two individual cells at the same aging conditions. That might be caused by not considered systematic errors or by random errors like the cell-to-cell variation of the single cells. Due to a delay in the third characterization step, the second measurement interval at 23 °C had to be extended from two to three months.

As expected, the capacity loss is higher at elevated temperature. Furthermore, there are differences between the capacity losses at various storage SOC. It is noticeable, that a higher SOC does not necessarily correlate with a higher capacity loss at time t. Although the loss of capacity is lowest at 50% SOC, it is almost the same in the long term at 70% and 90% SOC. At 23 °C, the capacity loss of one cell at 70% SOC is nearly twice as high compared to the 90% SOC cells after 422 days. However, this seems to be a single cell behavior since the second cell aged at 70% SOC has a similar capacity loss as the cells aged at 90% SOC.

After the first initial increase, the capacity loss flattens out at 40 °C and reaches a value of around 1% after 200 days. Subsequently, the curve turns into an exponential growth. In contrast, the capacity loss at 23 °C increases more linearly towards the end of the test series. At the beginning of the aging a negative capacity loss, which means a gain in capacity, was recorded. For one of the cells aged at 50% SOC, the phase of capacity gain is not finished even after more than one year of aging.

An initial gain in capacity was already observed in various calendar aging studies and is often explained by the passive anode effect [7,8,10]. To estimate the maximum PAE, the volumetric excess of the anode was determined in an initial cell opening. Each anode has a 5.2% larger volume than the corresponding cathode. Therefore, assuming equal volumetric capacity of the electrodes, a maximum of 5.2% of the

cell capacity could be stored in the overhang. To estimate how much of this capacity can be absorbed or released in the first calendar aging phases, it is assumed that the passive and active parts of the anode are in equilibrium at the beginning of the aging tests and that their SOC corresponds to the initial cell state of charge of 50% SOC. Accordingly, the overhang absorbs lithium ions at subsequent calendar aging at a higher SOC. The SOC of the overhang slowly equalizes to the SOC of the active anode during calendar aging. Therefore, for the calendar aging at 90% SOC, it is assumed, that the overhang SOC changes by a maximum of 40% SOC, which corresponds to a fraction of 2.1% of the total cell capacity. Storage at lower SOC has a correspondingly lower maximum capacity loss due to the overhang effect: 1% of the total cell capacity at 70% storage SOC in calendar aging and 0% capacity loss at 50% storage SOC. Thus, when stored at 50% SOC, a negligible loss or gain in capacity due to the PAE is expected. Since the battery cells were characterized only every two months, the main capacity loss due to PAE should occur in the first one to two calendar ageing phases. This does not agree with the measured capacity gain at 50% SOC which for one cell increases even further towards the end of the aging. Additionally, even the cells aged at higher SOC and 23 °C do not show an increased capacity loss in the first months of aging. This is not in agreement with the estimated maximum effect of the PAE. For this reason, the PAE does not provide an explanation for the observed aging behavior, in particular the capacity gain of the cells aged at 23 °C. There must be another superimposed effect.

3.2. Quantification of the characterization measurement effect

A periodic characterization measurement is used to quantify the capacity loss due to characterization $C_{loss,char}$. It is then separated from the capacity loss due to calendar aging, which can be divided into an irreversible part $C_{loss,cal,ir}$ (mainly SEI formation), and a reversible part $C_{loss,cal,rev}$ (e.g. capacity loss or gain through PAE). Consequently, the measured capacity loss in calendar aging adds up as follows

$$C_{loss,meas} = C_{loss,cal,ir} + C_{loss,cal,rev} + C_{loss,char}. \quad (6)$$

A capacity gain is a negative capacity loss and thus compensates capacity loss in the calendar aging measurement. Fig. 3a shows the capacity loss and Fig. 3b the discharge polarization resistance at 10% SOC over the number of characterizations of the two studied cells in the periodic characterization measurement. The resistance evaluation is done according to Eq. (1) ten seconds after the pulse. The SOC of 10% was chosen because the resistance is highest here and changes in resistance are best identifiable.

The capacity loss is negative at all characterizations which means that the capacity increases compared to the initial capacity. The capacity gain is a maximum of 0.8% of the initial capacity after seven characterizations. Subsequently, the capacity decreases linearly by approx. 0.3% up to the 15th characterization. Since all the results of the calendar aging at 23 °C up to 300 days after the start of the tests are less than 0.5% capacity loss (Fig. 2), the influence of the characterization on the capacity is not negligible small. Furthermore, in Fig. 3b, the resistance decreases with the number of characterizations. The effect of characterization equally affects all cells in the calendar aging measurement and therefore explains a drop in resistance independent of the aging SOC and temperature. Consequently, the influence of the characterization measurement can explain the resistance decrease observed by Naumann et al. [10] and Lewerenz et al. [19].

A capacity gain in combination with the drop in resistance during cyclic aging was already observed by Dubarry et al. [25] at LFP high energy cells. The capacity gain is explained by a reduced overvoltage at cyclization, which causes the discharge to terminate later, increasing the capacity of the cell. This could be the result of a reduced polarization resistance. Possible causes for a reduced polarization resistance include an improvement in the electronic conduction in the electrode material, a reduction in the charge transfer resistance at the interface

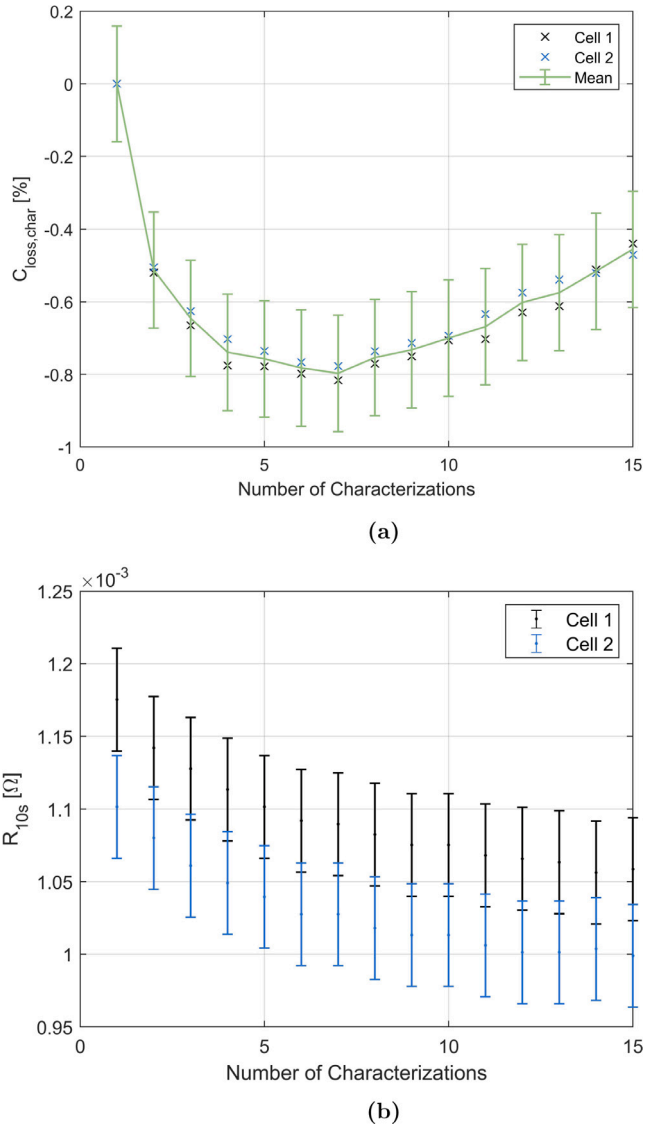

Fig. 3. Capacity loss (a) and resistance at 10% SOC (b) over the number of characterizations in the periodic characterization measurement.

between the electrode and the electrolyte, and an improvement in the diffusion of lithium ions through the active material and the electrolyte. Furthermore, an increase of the electrode surface and thus a decrease of the effective local current density at the same C-rate is a possible mechanism to reduce the overpotential at the corresponding electrode. Dubarry et al. [25] determined the increase of the cathode surface to be the most relevant mechanism which ultimately leads to an increase in capacity of the LFP cells considered. The influence of a kinetic effect in the periodic characterization measurement can be investigated analyzing the End Of Discharge Open Circuit Voltage (EOD OCV). Fig. 4a shows the EOD OCV 30 min after the battery is discharged with 1C and C/10 over the number of characterization cycles. The EOD OCV after discharge with 1C is significantly higher than after discharge with C/10. A higher open circuit voltage generally means a higher state of charge of the battery. Thus, the cell was discharged less at 1C discharge due to the higher voltage drop on the polarization resistance.

The relative EOD OCV for a discharge with 1C and C/10 is shown in Fig. 4b. At both current rates the EOD OCV reduces with the number of characterizations. The decrease at C/10 is about 0.5% after 15 characterizations while at 1C it is three times larger. A decreasing EOD OCV indicates a deeper discharge of the cell, which in turn is

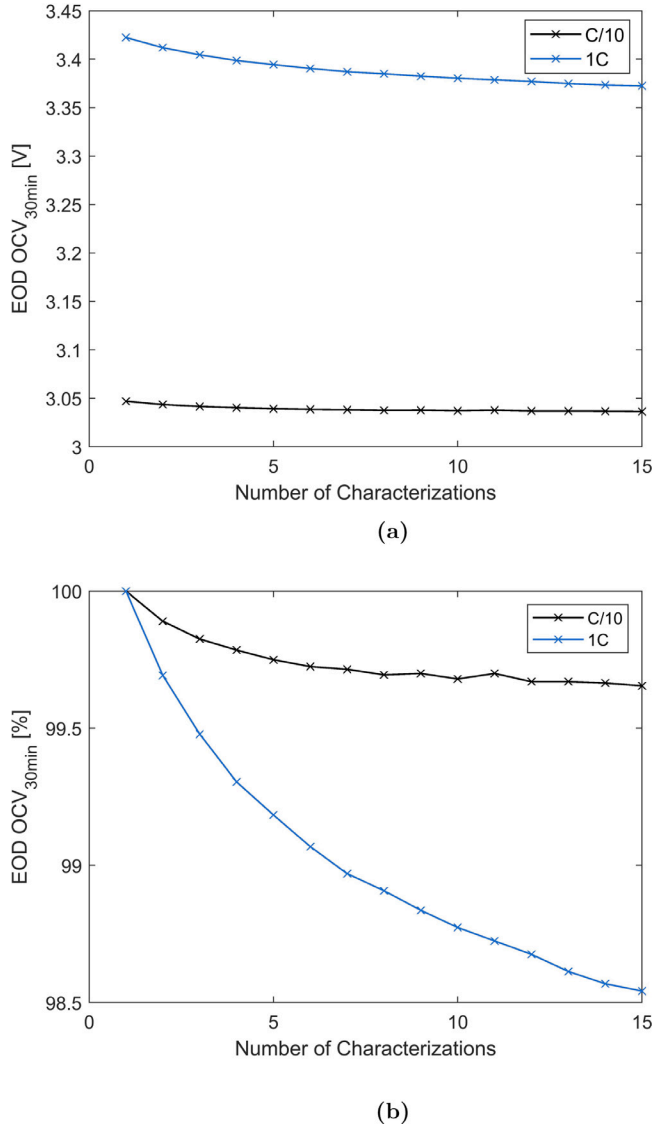

Fig. 4. End Of Discharge Open Circuit Voltage (EOD OCV) (a) and relative EOD OCV (b) 30 min after discharge with 1C and C/10 plotted over the number of characterizations in the periodic characterization measurement.

connected to an increase in capacity. Since the voltage losses on the polarization resistance rise with higher current rates, the decreasing resistance has a stronger influence on the capacity measurement carried out with a higher current and the capacity gain is more prominent here. This also supports the results of Hahn et al. [7] who found a smaller increase in capacity in the C/10 comparing to the 1C capacity measurement results. To reduce the influence of kinetic effect on the capacity measurement and to limit the aging due to the characterization itself, a capacity measurement with a smaller current is preferable to a 1C capacity measurement. The current rate of C/3 offers a good compromise between reducing measurement time and minimizing the effect of the characterization measurement. It is, next to 1C, the most recommended current rate to be used in the capacity measurement by test standards and research community [15].

The influence of the characterization measurement is not equally strong in all battery cell chemistries. High-power cells, for example, are less affected by kinetic effects since they are optimized for high power capability [25].

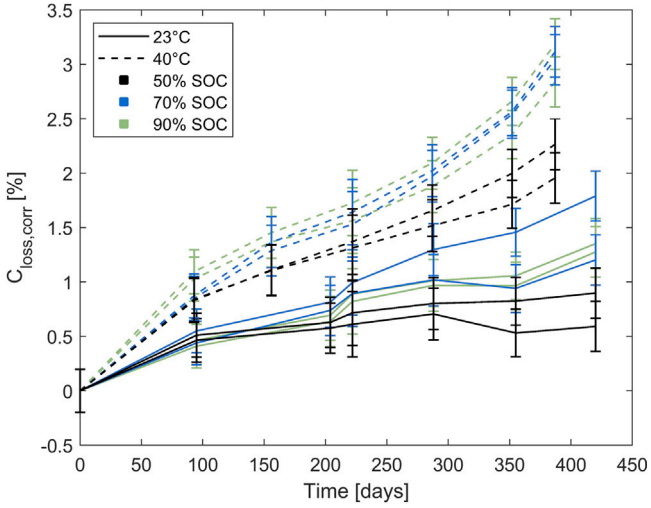

Fig. 5. Capacity loss in calendar aging corrected by the capacity loss due to characterization as a function of time.

3.3. Correction of the measurement data by the effect of characterization

To correct the effect of characterization on the capacity in calendar aging, the mean value of the measured capacity loss during characterization is subtracted from the capacity loss measured in the calendar aging study. According to Eq. (6) the result is the superposition of the reversible and irreversible capacity loss in calendar aging. The corrected capacity loss $C_{loss,corr}$ is shown in Fig. 5. The error of $C_{loss,corr}$ is determined over Pythagorean addition of the errors of $C_{loss,meas}$ and $C_{loss,char}$.

The correction provides a significant change in the calendar aging capacity loss. In contrast to the original capacity loss of the calendar aging measurement in Fig. 2, the typical flattening capacity loss with the time occurs at 23 °C instead of the (initial) capacity gain. Since the correction is independent of SOC and temperature in calendar aging, the previously recognized basic relationships (1. higher temperature causes more capacity loss, 2. lower capacity loss at 50% SOC than at 70% and 90% SOC) remain. The increase in capacity loss with longer test times is weakened and can now be seen from approximately 290 days on. As the effect is more noticeable at high temperatures and high SOC, it could be attributed to dissolution of transition metals at the cathode which deposit at the anode and accelerate SEI growth. Since we focus on the effect of the characterization, the reversible and irreversible capacity loss are not further separated and analyzed in this paper. Nevertheless, the contribution of the overhang to the initial increase in capacity loss could be estimated from the data using the method presented by Lewerenz et al. [20]. According to their theory the initial capacity loss is caused by the influence of the anode overhang and the following linear capacity loss belongs to the irreversible battery aging.

3.4. Model parameterization

The corrected data are now used to parameterize a semi-empirical aging model. For simplification, the functions depending on time, temperature and SOC are assumed to be independent of each other. The separated functions are first parameterized individually and then combined into an overall model.

3.4.1. Time dependency

For models with few fit parameters, the simple power law t^{β} time dependency approach provides a good compromise between high quality of the fit and low overfitting potential [7]. Describing the capacity

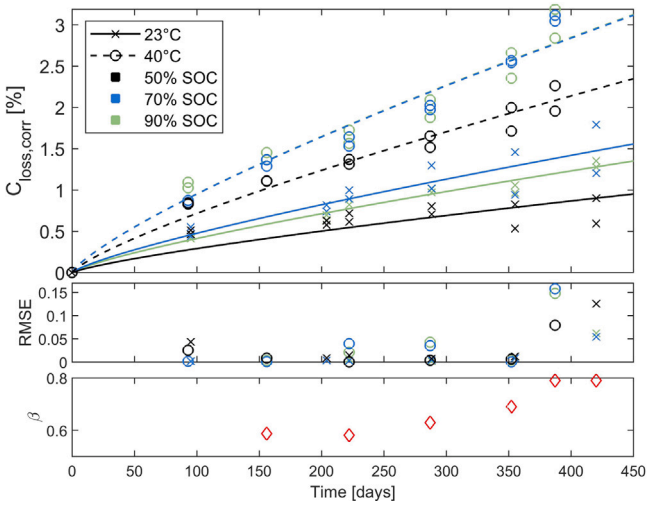

Fig. 6. Top: Fit (line) of the measured capacity loss at different SOC and temperatures (marker) over the time with the final exponent $\beta = 0.789$. Middle: Root Mean Squared Error (RMSE) of the model up to time t. Bottom: Model exponent β when fitting data up to time t.

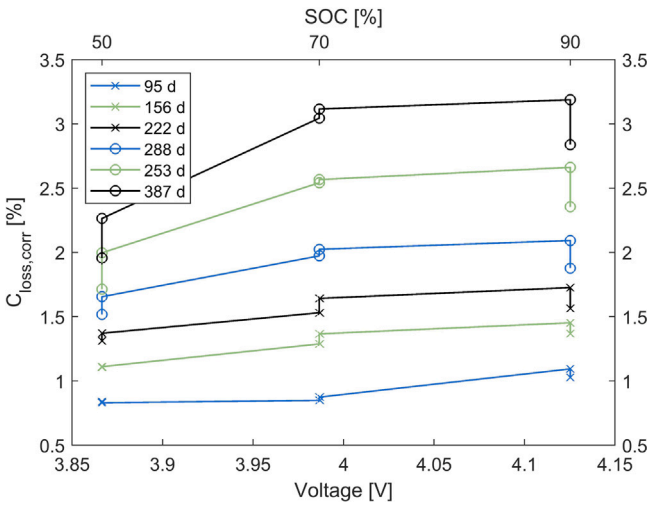

Fig. 7. Corrected capacity loss at 40 °C as a function of SOC at different times of the aging process.

loss due to SEI growth, this approach assumes that there is no SEI at time t = 0. Furthermore, the predicted capacity loss at infinite test time is infinite. To determine the exponent β of the time dependency, all measured data are fitted with the equation

$$C_{loss,corr}(SOC,T,t) = A(SOC,T)\cdot t^{\beta},\ 0<\beta<1. \tag{7}$$

The factor A(SOC,T) is determined individually for each measured temperature and SOC combination, using the mean of the capacity loss of the two aged cells. The parameter β is set to be the same for all measured data. The fitting is based on the least squares method and performed using Matlab. To find a minimum sum of the squares of the residuals, the initial value of A(SOC,T) is varied in ten steps between 0.1 and 1. The results of the fit are shown in Fig. 6. The factor A(T,SOC) is the same here for 70% and 90% SOC at 40 °C, so only one dashed line is visible. Furthermore, in the first subplot the Root Mean Squared Error (RMSE) for the deviation of the measurements mean value from the model is shown. Below this, the exponent β that results from fitting the data up to time t is plotted. It was determined from a minimum of three measured values.

For the cells considered, the final model exponent is $\beta = 0.789$. It provides a compromise between the initial root-shaped calendar aging and the long-term increasing capacity loss. Fitting only data up to 220 days, β is 0.581 which is close to the square root of time dependency typical for the diffusion limited SEI growth during storage [27]. The continuously increasing exponent due to the subsequent stronger increase in capacity loss demonstrates a change in aging behavior of the cells. The final exponent provides an underestimation of the capacity loss in the first months of aging. Nevertheless, the RMSE of the model is below 0.05 for all measurements up to 350 days, which is considered to be sufficient. Afterwards, the RMSE increases significantly. The changed aging behavior, especially at high temperature and high SOC, might be due to the influence of coupled reactions between the cathode and the anode since transition metal dissolution is accelerated by high temperatures and high SOC [17]. The measurements had to be stopped after 420 days, therefore it was not possible to investigate whether this effect only occurs in the short term or continues in the long term.

3.4.2. Temperature dependency

The temperature dependency is modeled by the Arrhenius equation. It characterizes the change in reaction kinetics with temperature and has already been used in many aging models [5–7]. The temperature-dependent capacity loss is described by

$$C_{loss,corr}(T,t) = \alpha\cdot\exp\left(\frac{-E_a}{R\cdot T}\right)\cdot t^{0.789} \tag{8}$$

with the ideal gas constant R and the activation energy E_a. The model parameters are α and E_a. To parameterize the temperature dependency, a reference SOC must be selected. The lowest RMSE of the model compared measured data at a fixed SOC and different temperatures is observed at 50% SOC. For this reason, 50% SOC is chosen as the reference SOC. Furthermore, by fitting the entire data, the lowest mean RMSE of the resulting model is achieved. If the SOC and temperature dependency would have to be evaluated at specific points in time, the best model results are obtained by using the latest possible date. However, hereby a change in aging behavior during long-term measurements should be considered. The model parameters E_a and α resulting from the fit are listed in Table 4.

3.4.3. SOC dependency

The capacity loss dependency on the SOC is evaluated at 40 °C. The cells capacity losses are more clearly distinguishable at elevated temperature. The SEI growth at the anode is strongly dependent on the anode potential [17]. Thus it is also dependent on the SOC of the cell, provided that there is no shift of the electrode potentials relative to each other. Next to SEI growth, the capacity loss during calendar aging can be influenced by cathode and coupled side reactions. Their quantity and SOC dependence varies with the cathode material and electrolyte composition [22]. Consequently, it is difficult to assume a fixed SOC dependency since various behaviors are possible at different cell chemistries for the same aging conditions. Therefore, an analysis of the SOC dependency is performed. For this purpose, Fig. 7 shows the corrected capacity loss versus SOC at constant temperature of 40 °C and fixed points in time.

First, the capacity loss increases linearly with higher SOC. The aging behavior changes after around 288 days. The capacity loss increases more strongly towards 70% SOC and then stagnates to 90% SOC. Due to increasing side reactions at the cathode at higher SOC, lithium ions intercalate back into the cathode. This may compensate capacity loss above 70% SOC and could be a cause for the apparently decreasing capacity loss at 90% SOC [11]. The increase in capacity loss between 50% and 70% SOC (which can also be seen in the exponential increase of the capacity loss at higher SOC in Fig. 5) could be due to transition metals coming from the cathode, accelerating SEI growth at the anode.

Table 4
Model parameters determined by fitting the corrected calendar aging data.

E_a [kJ/mol]	α	β	γ	δ
36.36	$2.15 \cdot 10^4$	0.789	$1.19 \cdot 10^{-4}$	0.01

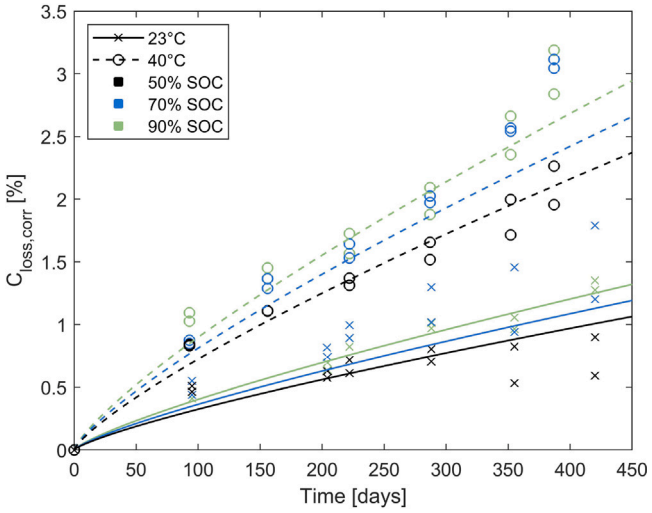

Fig. 8. Calendar aging model results for the SOC- and temperature-dependent capacity loss over the time (line) and corrected capacity loss data (marker).

These assumptions would need to be verified in a post-mortem analysis. Below 288 days, a linear SOC dependency can be assumed:

$$C_{loss,corr}(SOC,t) = (\gamma \cdot SOC + \delta) \cdot t^{0.789}. \quad (9)$$

The parameter γ and δ resulting from the fit of the total measured data at 40 °C are shown in Table 4.

3.4.4. Total calendar aging model

The separated functions for the capacity loss dependent on SOC and temperature are finally combined into an overall model. For this purpose, a scaling of the functions (8) and (9) is performed according to Schmalstieg et al. [1]:

$$C_{loss,corr}(T,SOC,t) = \frac{C_{loss,corr}(SOC,t) \cdot C_{loss,corr}(T,t) \cdot C_{loss,corr,\varnothing}}{C_{loss,corr}(50\%\ SOC,t) \cdot C_{loss,corr}(40\,°\mathrm{C},t)} \quad (10)$$

with the mean value of the SOC- and temperature-dependent functions at the reference SOC (50% SOC) and reference temperature (40 °C)

$$C_{loss,corr,\varnothing} = \frac{C_{loss,corr}(50\%\ SOC,t) + C_{loss,corr}(40\,°\mathrm{C},t)}{2}. \quad (11)$$

The model results are shown in Fig. 8. At the beginning and at the end of the measurement, the final model shows larger deviations from the capacity loss of the considered NMC cells. This is due to the changing aging behavior from approximately 288 days on. The selected time dependency according to the power law approach forms a compromise between early and long-term aging. The SOC dependency was parameterized on the basis of a linear relationship, which changes to a flattening SOC relationship in the course of the aging process. In future calendar aging models the changing aging behavior should be considered separately to increase model accuracy. Rumberg et al. [11] included the effect of cathodic side reactions in their calendar aging model. To the authors' knowledge, the influence of transition metal dissolution has not yet been considered in semi-empirical calendar aging models. This is part of future research.

4. Conclusion

In this calendar aging study on commercial NMC cells, additional periodic characterization measurements were used to quantify and correct the effect of the checkup on the loss of capacity due to calendar aging. A gain in capacity due to the characterization measurement has been detected. It was attributed to an improvement in cell kinetics which was indicated by a decrease in cell resistance. Due to the decreasing resistance, the end-of-discharge voltage is reached later, the cell is discharged further and the capacity increases. A stronger discharge of the cell was proven by the evaluation of the end of discharge open circuit voltage. Based on literature research, the cause of the decreasing resistance was assigned to an increase of the cathode surface due to cracking and structural disordering. The capacity gain caused by the kinetic effect and the electrode degradation itself increase with increasing current rate in the capacity measurement cycles. To ensure that the capacity fade results of future aging studies are comparable, the findings lead to the recommendation to perform the capacity measurement in cell characterizations with a lower current rate than 1C. The current rate of C/3, already often used in literature, provides a good compromise between saving measurement time and gentle cycling. The corrected measurement data showed the typical root-shaped capacity loss expected from SEI growth in the first nine months of aging. Subsequently, a change in the aging behavior has been found. It was characterized by an exponential increase in capacity loss over time, especially at elevated temperature and SOC. Furthermore, a constant capacity loss was observed between 70% SOC and 90% SOC instead of a previous linear SOC dependency. This may be attributed to the influence of cathodic and coupled side reactions. The exact cause of the changed aging behavior would have to be further analyzed, for example by a post-mortem analysis. Finally, the corrected calendar aging data were successfully used to parameterize a semi-empirical calendar aging model for the capacity loss. The presented aging model is well suited for an estimation of calendar aging. Nevertheless, for a more detailed capacity loss model, the change in the aging behavior of the batteries with long-term aging should be addressed in future investigations.

CRediT authorship contribution statement

Amelie Krupp: Conceptualization, Methodology, Software, Validation, Formal analysis, Data curation, Visualization, Writing – original draft, Writing – review & editing. **Robert Beckmann:** Conceptualization, Methodology, Software, Formal analysis, Supervision, Writing – original draft, Writing – review & editing. **Theys Diekmann:** Investigation, Resources, Writing – review & editing, Funding acquisition. **Ernst Ferg:** Conceptualization, Methodology, Supervision, Writing – review & editing. **Frank Schuldt:** Conceptualization, Resources, Supervision, Writing – review & editing, Funding acquisition. **Carsten Agert:** Conceptualization, Resources, Supervision, Writing – review & editing.

Declaration of competing interest

The authors declare that they have no known competing financial interests or personal relationships that could have appeared to influence the work reported in this paper.

Acknowledgments

The results were generated in the framework of the project HyReK 2.0 (grant no. 03ET6147C). We thank the German Federal Ministry for Economic Affairs and Energy (BMWi) for funding.

References

[1] J. Schmalstieg, S. Käbitz, M. Ecker, D.U. Sauer, A holistic aging model for Li(NiMnCo)O2 based 18650 lithium-ion batteries, J. Power Sources 257 (2014) 325–334, http://dx.doi.org/10.1016/j.jpowsour.2014.02.012.

[2] X. Jin, A. Vora, V. Hoshing, T. Saha, G. Shaver, O. Wasynczuk, S. Varigonda, Applicability of available Li-ion battery degradation models for system and control algorithm design, Control Eng. Pract. 71 (2018) 1–9, http://dx.doi.org/10.1016/j.conengprac.2017.10.002.

[3] B. Xu, A. Oudalov, A. Ulbig, G. Andersson, D.S. Kirschen, Modeling of Lithium-Ion battery degradation for cell life assessment, IEEE Trans. Smart Grid 9 (2) (2018) 1131–1140, http://dx.doi.org/10.1109/TSG.2016.2578950.

[4] I. Baghdadi, O. Briat, J.-Y. Delétage, P. Gyan, J.-M. Vinassa, Lithium battery aging model based on Dakin's degradation approach, J. Electrochem. Soc. 325 (2016) 273–285, http://dx.doi.org/10.1016/j.jpowsour.2016.06.036.

[5] M. Ecker, J.B. Gerschler, J. Vogel, S. Käbitz, F. Hust, P. Dechent, D.U. Sauer, Development of a lifetime prediction model for lithium-ion batteries based on extended accelerated aging test data, J. Power Sources 215 (2012) 248–257, http://dx.doi.org/10.1016/j.jpowsour.2012.05.012.

[6] S. Grolleau, A. Delaille, H. Gualous, P. Gyan, R. Revel, J. Bernard, E. Redondo-Iglesias, J. Peter, Calendar aging of commercial graphite/LiFePO4 cell – Predicting capacity fade under time dependent storage conditions, J. Electrochem. Soc. 255 (2014) 450–458, http://dx.doi.org/10.1016/j.jpowsour.2013.11.098.

[7] S.L. Hahn, M. Storch, R. Swaminathan, B. Obry, J. Bandlow, K.P. Birke, Quantitative validation of calendar aging models for lithium-ion batteries, Electrochem. Solid-State Lett. 400 (2018) 402–414, http://dx.doi.org/10.1016/j.jpowsour.2018.08.019.

[8] J. de Hoog, J.-M. Timmermans, D. Ioan-Stroe, M. Swierczynski, J. Jaguemont, S. Goutam, N. Omar, J. van Mierlo, P. van den Bossche, Combined cycling and calendar capacity fade modeling of a Nickel-Manganese-Cobalt Oxide Cell with real-life profile validation, Appl. Energy 200 (2017) 47–61, http://dx.doi.org/10.1016/j.apenergy.2017.05.018.

[9] A. Marongiu, M. Roscher, D.U. Sauer, Influence of the vehicle-to-grid strategy on the aging behavior of lithium battery electric vehicles, Appl. Energy 137 (2015) 899–912, http://dx.doi.org/10.1016/j.apenergy.2014.06.063.

[10] M. Naumann, M. Schimpe, P. Keil, H.C. Hesse, A. Jossen, Analysis and modeling of calendar aging of a commercial LiFePO4/graphite cell, J. Energy Storage 17 (2018) 153–169, http://dx.doi.org/10.1016/j.est.2018.01.019.

[11] B. Rumberg, B. Epding, I. Stradtmann, M. Schleder, A. Kwade, Holistic calendar aging model parametrization concept for lifetime prediction of graphite/NMC lithium-ion cells, J. Energy Storage 30 (2020) 101510, http://dx.doi.org/10.1016/j.est.2020.101510.

[12] K. Smith, M. Earleywine, E. Wood, J. Neubauer, A. Pesaran, Comparison of plug-in hybrid electric vehicle battery life across geographies and drive cycles, in: SAE Technical Paper Series, in: SAE Technical Paper Series, SAE International400 Commonwealth Drive, Warrendale, PA, United States, 2012, http://dx.doi.org/10.4271/2012-01-0666.

[13] T. DuBeshter, J. Jorne, Pulse polarization for li-ion battery under constant state of charge: Part I. Pulse discharge experiments, J. Electrochem. Soc. 164 (11) (2017) E3539–E3546, http://dx.doi.org/10.1149/2.0551711jes.

[14] A. Barai, K. Uddin, W.D. Widanage, A. McGordon, P. Jennings, A study of the influence of measurement timescale on internal resistance characterisation methodologies for lithium-ion cells, Sci. Rep. 8 (1) (2018) 21, http://dx.doi.org/10.1038/s41598-017-18424-5.

[15] A. Barai, K. Uddin, M. Dubarry, L. Somerville, A. McGordon, P. Jennings, I. Bloom, A comparison of methodologies for the non-invasive characterisation of commercial Li-ion cells, Prog. Energy Combust. Sci. 72 (2019) 1–31, http://dx.doi.org/10.1016/j.pecs.2019.01.001.

[16] G. Mulder, N. Omar, S. Pauwels, M. Meeus, F. Leemans, B. Verbrugge, W. de Nijs, P. van den Bossche, D. Six, J. van Mierlo, Comparison of commercial battery cells in relation to material properties, Electrochim. Acta 87 (2013) 473–488, http://dx.doi.org/10.1016/j.electacta.2012.09.042.

[17] P. Keil, A. Jossen, Calendar aging of NCA Lithium-Ion batteries investigated by differential voltage analysis and Coulomb tracking, J. Electrochem. Soc. 164 (1) (2017) A6066–A6074, http://dx.doi.org/10.1149/2.0091701jes.

[18] B. Gyenes, D.A. Stevens, V.L. Chevrier, J.R. Dahn, Understanding anomalous behavior in Coulombic efficiency measurements on li-ion batteries, J. Electrochem. Soc. 162 (3) (2015) A278–A283, http://dx.doi.org/10.1149/2.0191503jes.

[19] M. Lewerenz, J. Münnix, J. Schmalstieg, S. Käbitz, M. Knips, D.U. Sauer, Systematic aging of commercial LiFePO 4 |Graphite cylindrical cells including a theory explaining rise of capacity during aging, Electrochem. Solid-State Lett. 345 (2017) 254–263, http://dx.doi.org/10.1016/j.jpowsour.2017.01.133.

[20] M. Lewerenz, G. Fuchs, L. Becker, D.U. Sauer, Irreversible calendar aging and quantification of the reversible capacity loss caused by anode overhang, J. Energy Storage 18 (2018) 149–159, http://dx.doi.org/10.1016/j.est.2018.04.029.

[21] R.D. Deshpande, D.M. Bernardi, Modeling solid-electrolyte interphase (SEI) fracture: Coupled mechanical/chemical degradation of the lithium ion battery, J. Electrochem. Soc. 164 (2) (2017) A461–A474, http://dx.doi.org/10.1149/2.0841702jes.

[22] J.P. Pender, G. Jha, D.H. Youn, J.M. Ziegler, I. Andoni, E.J. Choi, A. Heller, B.S. Dunn, P.S. Weiss, R.M. Penner, C.B. Mullins, Electrode degradation in lithium-ion batteries, ACS Nano 14 (2) (2020) 1243–1295, http://dx.doi.org/10.1021/acsnano.9b04365.

[23] M.M. Kabir, D.E. Demirocak, Degradation mechanisms in Li-ion batteries: a state-of-the-art review, Int. J. Energy Res. 41 (14) (2017) 1963–1986, http://dx.doi.org/10.1002/er.3762.

[24] L. von Kolzenberg, A. Latz, B. Horstmann, Solid-electrolyte interphase during battery cycling: Theory of growth regimes, ChemSusChem (2020) http://dx.doi.org/10.1002/cssc.202000867.

[25] M. Dubarry, C. Truchot, B.Y. Liaw, Cell degradation in commercial LiFePO4 cells with high-power and high-energy designs, Electrochem. Solid-State Lett. 258 (2014) 408–419, http://dx.doi.org/10.1016/j.jpowsour.2014.02.052.

[26] Fundamentals of metrology: Part 4: Evaluation of measurements; uncertainty of measurement.

[27] F. Single, A. Latz, B. Horstmann, Identifying the mechanism of continued growth of the solid-electrolyte interphase, ChemSusChem 11 (12) (2018) 1950–1955, http://dx.doi.org/10.1002/cssc.201800077.